Numerical modelling of concrete beams at serviceability conditions with a discrete crack approach and non-iterative solution-finding algorithms

D. Dias-da-Costa
School of Civil Engineering, The University of Sydney, Australia

R. N. F. do Carmo
CERIS, Polytechnic Institute of Coimbra, Portugal

R. Graça-e-Costa
CEPAC, Department of Civil Engineering, University of Algarve, Portugal

ABSTRACT: This paper describes the development and validation of a comprehensive numerical model enabling the simulation of reinforced concrete beams at serviceability conditions using a discrete crack approach. The highly non-linear behaviour introduced by the different material models and the multiple cracks localising and propagating within the member pose a challenging task to classic iterative solvers, which often fail to converge. This limitation is solved with a non-iterative solution-finding algorithm, in which a total approach is used to overcome critical bifurcation points. The finite element model is validated using experimental data concerning lightweight aggregate concrete beams under flexural loading. The model is shown to properly simulate both overall and particular features of the structural response, including curvature, crack openings and crack patterns. The model is then applied to carry out a small parametric study on the role of the longitudinal reinforcement ratio and crack widths in reinforced concrete beams.

1 INTRODUCTION

Estimating the real stiffness of a partially fractured concrete member for a given design load is a very difficult task, in particular because the concrete placed between cracks has a significant role in transferring tensile stresses – this is usually known as the 'tension stiffening effect' – and the crack pattern can be random and it also depends on the maximum load the structure experienced. For this reason, predicting the behaviour of a concrete member subjected to serviceability loads, and corresponding crack openings and overall deformation, can encompass several difficulties. In the last decades, the research community has witness many computational approaches to be introduced for predicting the fractured behaviour of different materials with the discrete representation of cracks. There are now different numerical techniques that can be used. Advanced techniques, for instance, are able to avoid the need for remeshing when cracks propagate by making use of enriched finite element meshes (nodes or elements) that can simulate the discontinuous displacement fields associated with cracks (Belytschko & Black, 1999, Moës et al., 1999, Wells & Sluys, 2001a, Areias & Belytschko, 2005, Dvorkin et al., 1990, Oliver, 1996, Jirásek & Zimmermann, 2001, Wells & Sluys, 2001b, Linder & Armero, 2007, Alfaiate et al., 2002, Dias-da-Costa et al., 2013). Although these advanced models are available, most validations have been focusing on the formulation itself and have used 'well-known' benchmark solutions, where the specimen usually fails under a limited number of highly localised cracks. In addition, comparison with experimental data is typically made using load vs. displacement curves, and other relevant features (e.g. crack openings) are missing. Aiming at contributing to reduce this gap, the authors herein present the validation of a numerical model for predicting the fractured behaviour of reinforced concrete members with discrete cracks for serviceability monotonic loads.

2 NUMERICAL MODELLING

2.1 *Discretised equations*

In quasi-brittle materials, the discontinuities are typically much softer than the bulk and its opening can be considered to be transmitted to the neighbouring material as if it were a rigid body movement. The stresses along the discontinuity are in equilibrium with the surrounding bulk, which unloads elastically as the discontinuity widens and softens its tensile stress. Under this assumption, it can be shown that the discretised set of equations for a finite element containing a crack is given by (Simo & Rifai, 1990, Dias-da-Costa et al., 2009, Dias-da-Costa et al., 2013, Dias-da-Costa et al., 2010):

$$\begin{bmatrix} \mathbf{K}^e_{\hat{a}\hat{a}} & -\mathbf{K}^e_{\mathbf{aw}} \\ -\mathbf{K}^e_{\mathbf{aw}} & \mathbf{K}^e_{\mathbf{ww}} + \mathbf{K}^e_d + \mathbf{K}^e_p \end{bmatrix} \begin{Bmatrix} \mathrm{d}\mathbf{a}^e \\ \mathrm{d}\mathbf{w}^e \end{Bmatrix} = \begin{Bmatrix} \mathrm{d}\hat{\mathbf{f}}^e \\ \mathrm{d}\tilde{\mathbf{f}}^e \end{Bmatrix} \quad (1)$$

where $\mathbf{K}^e_{\hat{a}\hat{a}} = \int_{\Omega^e \setminus \Gamma^e_d} \mathbf{B}^{eT} \mathbf{D}^e \mathbf{B}^e \, \mathrm{d}\Omega$ is the stiffness of a regular finite element, $\mathbf{B}^e$ is the strain-nodal displacement matrix, $\mathbf{D}^e$ is the linearised constitutive matrix for the bulk, $\mathbf{K}^e_d = \int_{\Gamma^e_d} \mathbf{N}^{eT}_w \mathbf{T}^e \mathbf{N}^e_w \, \mathrm{d}\Gamma$ is the stiffness of the discontinuity, $\mathbf{N}^e_w$ contains linear interpolation functions defined along the discontinuity, $\mathbf{T}^e$ is the linearised constitutive matrix for the discontinuity, $\mathbf{K}^e_p$ is a penalty matrix that enforces the shear jump transmission along the discontinuity, $\mathbf{K}^e_{\mathbf{aw}} = \mathbf{K}^e_{\hat{a}\hat{a}} \mathbf{H}^e_{\Gamma_d} \mathbf{M}^{ek}_w$, $\mathbf{K}^e_{\mathbf{wa}} = \mathbf{K}^{eT}_{\mathbf{aw}}$ and $\mathbf{K}^e_{\mathbf{ww}} = \left(\mathbf{H}^e_{\Gamma_d} \mathbf{M}^{ek}_w \right)^T \mathbf{K}^e_{\hat{a}\hat{a}} \mathbf{H}^e_{\Gamma_d} \mathbf{M}^{ek}_w$, $\mathbf{a}^e$ are the total displacements on the regular nodes of the element, $\mathbf{w}^e$ is a vector containing the opening of the discontinuity at both extremities over the edges of the element and $\hat{\mathbf{f}}^e$ are the regular forces. It can be shown that $\mathrm{d}\tilde{\mathbf{f}}^e = \mathrm{d}\mathbf{f}_w{}^e - \left(\mathbf{H}^e_{\Gamma_d} \mathbf{M}^{ek}_w \right)^T \mathrm{d}\hat{\mathbf{f}}^e$ is zero under certain circumstances.

2.2 *Solution procedure*

New crack fronts are introduced during the numerical analysis through the centre of each finite element whenever the first principal stress reaches the tensile strength of the material. In the same way, existing fronts are propagated when the first principal stress at the tip reaches the tensile strength of the material. The angle of propagation is orthogonal to the first principal stress and is kept constant during the analysis and after the onset of cracking. The additional nodes used to define the discontinuity within each element are global and shared among enriched neighbouring elements, hence assuring the continuity of jumps and tractions across edges.

The numerical solution is found using a non-iterative procedure that was shown to be robust in the presence of many sources of material non-linearities (e.g. concrete crushing, cracks opening, steel yielding, bond-slip in steel-concrete interfaces) (Graça-e-Costa et al., 2012). Before starting the analysis, all constitutive models are discretised into multilinear branches, hence avoiding the need to iterate at the constitutive level. Each step of analysis is composed of a trial step, followed by a true step.

The trial step starts with the load being applied to the structure and the selection of the solution sense leading to the highest energy release rate (Gutiérrez, 2004, Verhoosel et al., 2009). If no bifurcation points are found, meaning that all integration points follow admissible constitutive paths, the trial step becomes the true step and a new one is initiated. In the presence of bifurcation points, transition is made to a total approach such that damage grows on all material points that follow admissible paths and according to the information retrieved during the tentative step. A detailed description of the method can be found in (Graça-e-Costa et al., 2012, Graça-e-Costa et al., 2013).

3 EXPERIMENTAL TESTS

The experimental benchmark data used for validation purposes was obtained from two reinforced lightweight aggregate concrete (LWAC) beams loaded on two points and tested until failure. The beams were 3 m long and had a cross-section of 12 cm by 27 cm. Two different longitudinal tensile reinforcement ratios were adopted, respectively 1.12% (beam B1s-1.12T) and 2.96% (beam B1s-2.96T), to obtain two distinct behaviours under ultimate limit states (see Figure 1) with, respectively, under- and over-reinforced failure modes. The stirrups were 8 mm diameter and spaced 50 mm. The bars adopted were ribbed and S 500, whereas the LWAC had a compressive strength of 57 MPa, a tensile strength of 4 MPa and a Young's modulus of 25.5 GPa.

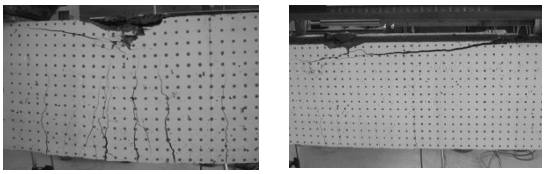

Figure 1. Under- and over-reinforced failure.

During the test, the beams were simply supported with 2.80 m between supports and loaded in two points at 40 cm from the mid-span. The typical load vs. mid-span curves can be seen in Figure 2, whereas Figure 3 shows the structural scheme.

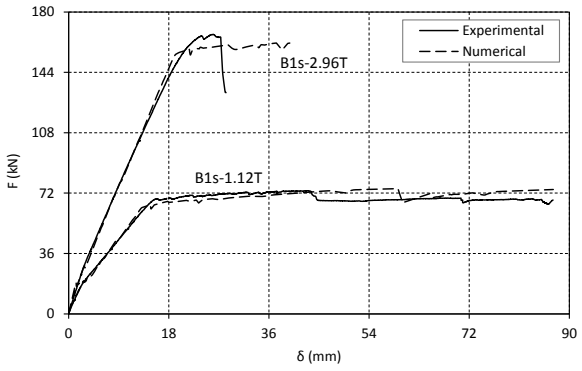

Figure 2. Load vs. mid-span displacement curves (Carmo et al., 2013).

4 VALIDATION

This section presents a detailed comparison between numerical and experimental results. Particular focus is given to deformations and crack patterns, since these are the most relevant for reinforced concrete structures under service limit states. With this aim, the analysis focuses the range between 60 and 80% of the maximum load supported by each beam.

The numerical model is defined in the assumption of plane stress, with the concrete being modelled using bilinear elements and the steel reinforcements being modelled using linear truss elements – see Figure 3. Interface elements simulate the bond between steel and concrete with the constitutive behaviour taken from the Model Code 2010 (fib, 2013). Steel is assumed to behave as elastic perfectly plastic in both tension and compression.

The constitutive model for concrete is linear elastic and perfectly plastic under compression, and linear elastic under tension. In the latter case, discontinuities are embedded to simulate cracked finite elements according to the procedure discussed in Section 2 and using a mode-I exponential softening law. Since the fracture energy was not experimentally assessed, a value of 0.10 N/mm was chosen having into account typical results.

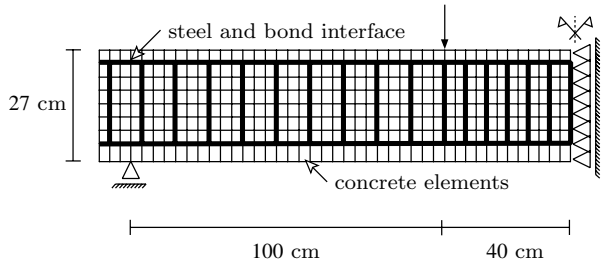

Figure 3. Structural scheme and mesh.

4.1 *Displacements, curvatures and critical loads*

Figure 2 shows the load vs. mid-span displacement for both beams until failure. There is a good overall agreement between numerical and experimental data, with the model predicting the response in the first (uncracked state) and second stages (cracked state). The cracking, yielding and maximum loads are also properly predicted, as shown by Figure 4, with the numerical model being sensitive to the role of the longitudinal reinforcement ratio on the response. The post-peak behaviour for the over-reinforced model, however, cannot be captured by the simulation due to the assumption of a perfect-plastic material made for concrete. This limitation, however, does not impact on the results since focus is given superficially to serviceability loads significantly below that threshold.

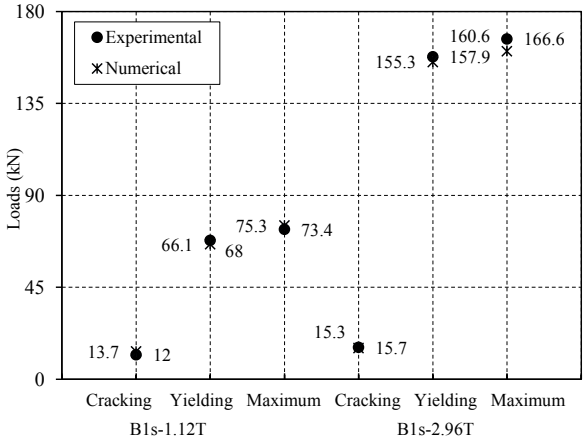

Figure 4. Cracking, yielding and maximum loads.

4.2 *Crack openings*

Figure 5 presents the sum of the widths of all the cracks in the region between applied loads and at the level of the longitudinal tensile reinforcements. This sum was selected to minimise the impact of the experimental randomness associated with cracking. The numerical results are generally close to the experimental observation for all stages of analysis, with differences found only for the last stage of the under-reinforced beam. This confirms the applicability of the model to predict crack openings, which is also related with the good agreement regarding the cracked flexural stiffness seen in Figure 2.

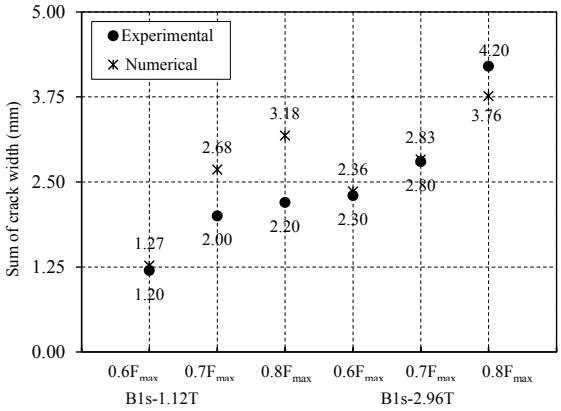

Figure 5. Crack openings for each reference load.

The numerical model allows extracting more data, in particular the evolution of the crack width with the average steel stress – see Figure 6. Initially, the crack width increases almost linearly with the steel stress. After the onset of steel yielding, the crack width progresses much faster due to the inability of the reinforcement in constraining the crack opening in that region. The relation between mid-span displacement and crack width is very interesting because it reveals different behaviours. The average crack width increases linearly with the displacements for all range of analysis, whereas the maximum crack width has two distinct stages. Before 20 mm, the rate is similar to the one observed on the average crack width, meaning that there are no criti-

cal cracks. After this stage, however, the rate increases substantially, clearly showing that there is at least one critical crack dominating the response. Even during this stage, the evolution is proportional to the overall displacement.

The crack pattern and stress distribution obtained with the numerical model is shown in Figure 7 for the over-reinforced beam. It is interesting to denote that the process of cracking is not yet stabilised at 60% of the ultimate load. The onset of cracking starts with the localisation of an active crack in the region where the stress is higher (underneath the applied load) – Figure 7 (top). As the distance to the crack increases, conditions can be met for another crack to form, as soon as the tensile strength of the bulk is reached by the stress bond transfer mechanism. Two new cracks then become active in Figure 7 at 28% of the maximum load. As the applied load is further increased, the stresses in the concrete between the cracks also increase progressively, until new cracks localise between the previously existing cracks – compare Figures 7 at 42% and 49% of the ultimate load. This ability to capture the process of crack localisation and the tension stiffening effect is critical to predict the behaviour under serviceability conditions.

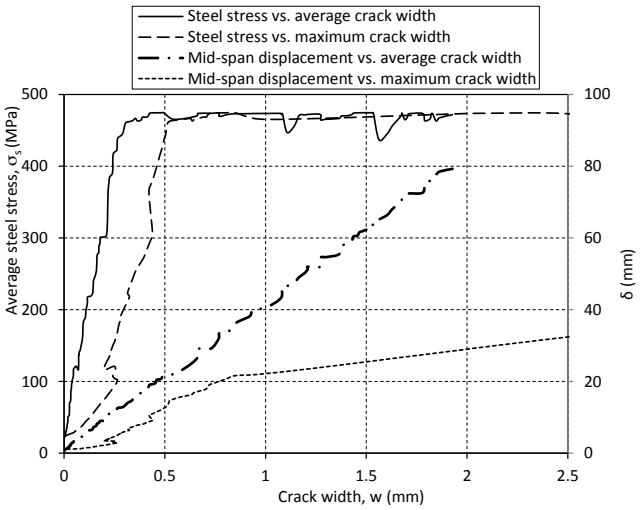

Figure 6. Average steel stress and displacement vs. maximum and average crack width for specimen B1s-1.12T

5 PARAMETRIC STUDY

Using the numerical model validated in the previous section, a parametric study is now undertaken to assess the impact of different tensile reinforcement ratios on the structural response. In all the analyses described next, the geometry, material properties and loading conditions are kept the same as in Section 3. Three additional models are defined to have a complete spectrum of tensile reinforcement ratios. The models with the highest and lowest ratios are close to the minimum and maximum allowed by the Eurocode 2. The corresponding tensile and compressive area of steel reinforcements and corresponding ratios are summarised in Table 1.

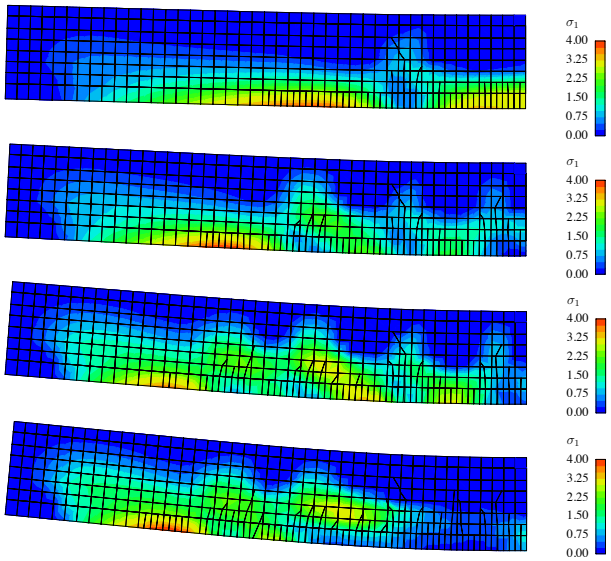

Figure 7. First principal stress and crack pattern for specimen B1s-2.96T at 17%, 28%, 42% and 49% of the ultimate load from top to bottom.

Table 1. Numerical models with different tensile reinforcement ratios.

Beam	A_s (cm^2)	d (cm)	$\rho=A_s/(bd)$ (%)	A_s' (cm^2)	$\rho'=A_s'/(bd)$ (%)
B1s-0.58T	1.57 (2∅10)	23.7	0.58	0.57 (2∅6)	0.20
B1s-1.12T	3.14 (4∅10)	23.4	1.12		
B1s-2.06T	5.59 (2∅16+2∅10)	23.0	2.06		
B1s-2.96T	8.04 (4∅16)	22.6	2.96		
B1s-4.63T	12.57 (4∅20)	22.2	4.63		

The load vs. mid-span displacement curves are shown in Figure 8. It is highlighted how the overall behaviour of all models and corresponding strength changes with the increasing longitudinal reinforcement ratio. The points represented in each curve identify the three stages selected for further analysis under serviceability conditions and for the same strength level regardless of the model, i.e. for 60, 70 and 80% of the maximum load. The impact of the tensile reinforcement ratio on the bending stiffness is seen more clearly in Figure 9, where the bending moment is related with the curvature at the central area of the beam (i.e., between applied loads). In this figure, the moment is calculated using the applied load, whereas the curvatures are provided by the second derivative of the parabolic curve adjusted to the vertical displacements between loads. The ratio between moment and curvature provides the flexural stiffness and this value is seen in the slope of the lines depicted in Figure 9. The stiffness at serviceability increases, as expected, with the reinforcement ratio, since there is an increasing area of reinforcement contributing for the moment of inertia. The in-

creasing reinforcement also decreases the magnitude of deformations, which is evident for the same load level.

The control of crack openings in reinforced concrete structures is very important, not only to assure a proper structural behaviour for serviceability loads, but also to achieve the required durability and acceptable appearance. The numerical model with discrete cracks is suitable to predict this behaviour, as shown by the evolution of the tensile stress in steel reinforcements with the maximum crack width represented Figure 10. This relation is almost linear for all the range of reinforcement ratios tested, with the highest ratios being related with the smaller crack widths. This is in agreement with what would be expected and confirms the approach often followed in design codes where crack openings are limited to acceptable values by constraining the stress level in steel reinforcements.

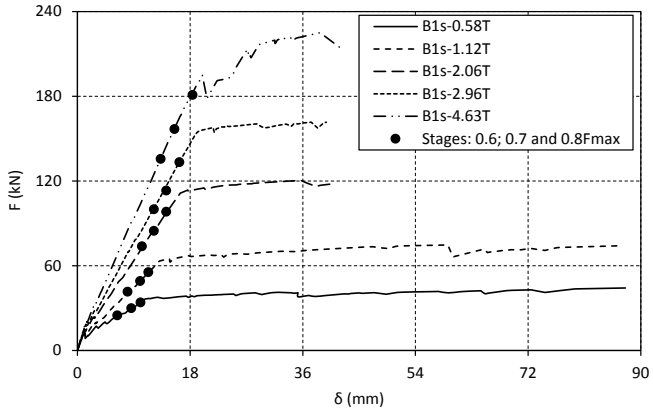

Figure 8. Load vs. mid-span displacement for all tensile reinforcement ratios.

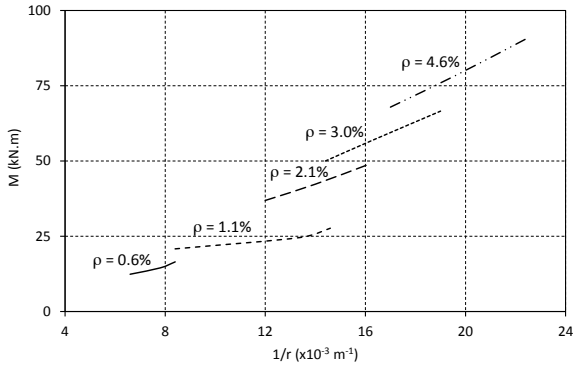

Figure 9. Moment vs. curvature for all tensile reinforcement ratios and loading stages.

Another parameter that can be analysed is the total crack opening per meter at the level of the tensile reinforcement. This parameter can be related with the durability of structure, since it provides indirect information about the possible area of steel exposed to the environment and to a higher risk of corrosion. This value also extends the information retrieved from the maximum crack width, which only gives meaningful data regarding a critical cross-section.

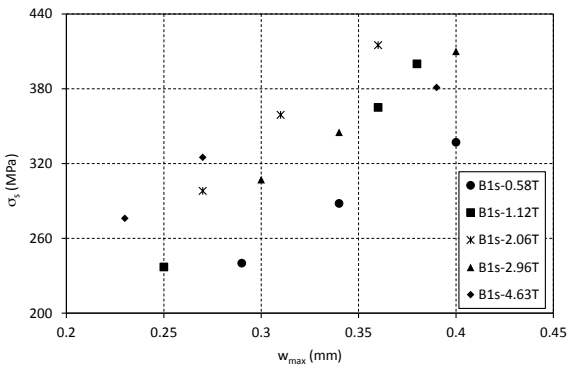

Figure 10. Steel stress vs. maximum crack opening.

The relation between tensile reinforcement ratio and the total crack opening per meter has an interesting trend. For the same level of strength and for steel ratios below 2.5%, the total opening of cracks decreases linearly with the reinforcement ratio. However, for ratios above 2.5%, the total crack opening almost does not change and there is no advantage in adopting higher ratios beyond this point solely with the purpose of reducing the exposure level of tensile steel reinforcements (Figure 11).

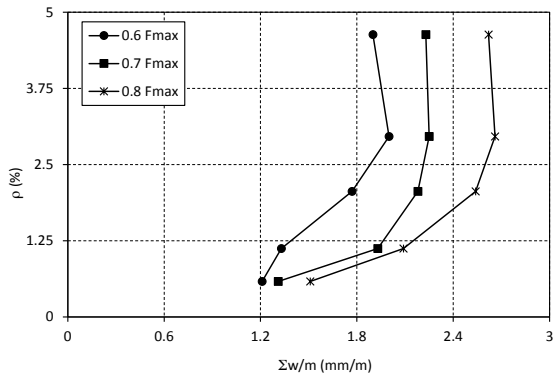

Figure 11. Reinforcement ratio vs. total crack opening per meter.

6 CONCLUSIONS

This paper presented and validated a computational framework within the scope of the discrete crack approach that can be used to efficiently predict the behaviour of concrete members for any level of loading. The model includes the discrete representation of cracks and embeds the rigid body movements associated with the opening of the cracks inside finite elements. A non-iterative algorithm is used to obtain the structural response, regardless of the numerous sources of material non-linearities that often compromises the convergence to a solution. Good agreement was observed between numerical and experimental results, including all meaningful parameters, such as cracking, yielding and ultimate loads.

Same observation extends to other parameters that are critical to the accurate prediction of the behaviour under serviceability monotonic loads. These parameters include the process of crack localisation and propagation, as well as the crack openings reported for the different levels of loading. Overall, it can be highlighted the good agreement between numerical and experimental data, including flexural cracked stiffness, crack openings and the tension-stiffening effect, all automatically incorporated in the simulations and evolving with the load level.

It is also worth highlighting that the tensile reinforcement ratio seems to be a significant parameter for controlling the total crack openings for tensile reinforcement ratios below 2.5%. Above this reference value, however, the total opening of the cracks remains nearly unchanged.

ACKNOWLEDGEMENTS

The first author would like to acknowledge the support from the Australian Research Council through its Discovery Early Career Researcher Award (DE150101703) and from the Faculty of Engineering & Information Technologies, The University of Sydney, under the Faculty Research Cluster Program. Acknowledgment is also extended to FCT (Portuguese Foundation for Science and Technology), through ISISE, under project UID/ECI/04029/2013.

REFERENCES

Alfaiate, J., Wells, G. N. & Sluys, L. J. 2002. On the use of embedded discontinuity elements with crack path continuity for mode-I and mixed-mode fracture. *Engineering Fracture Mechanics,* 69**,** 661-686.

Areias, P. M. A. & Belytschko, T. 2005. Analysis of three-dimensional crack initiation and propagation using the extended finite element method. *International Journal for Numerical Methods in Engineering,* 63**,** 760-788.

Belytschko, T. & Black, T. 1999. Elastic crack growth in finite elements with minimal remeshing. *International Journal for Numerical Methods in Engineering,* 45**,** 601-620.

Carmo, R. N. F., Costa, H., Simões, T., Lourenço, C. & Andrade, D. 2013. Influence of both concrete strength and transverse confinement on bending behavior of reinforced LWAC beams. *Engineering Structures,* 48**,** 329-341.

CEN 2004. EN 1992-1-1: Eurocode 2: Design of concrete structures - Part 1-1: General rules and rules for buildings. European Committee for Standardization (CEN).

Dias-da-Costa, D., Alfaiate, J., Sluys, L. J., Areias, P. & Júlio, E. N. B. S. 2013. An embedded formulation with conforming finite elements to capture strong discontinuities. *International Journal For Numerical Methods In Engineering,* 93**,** 224-244.

Dias-da-Costa, D., Alfaiate, J., Sluys, L. J. & Júlio, E. N. B. S. 2009. A discrete strong discontinuity approach. *Engineering Fracture Mechanics,* 76**,** 1176-1201.

Dias-da-Costa, D., Alfaiate, J., Sluys, L. J. & Júlio, E. N. B. S. 2010. A comparative study on the modelling of discontinuous fracture by means of enriched nodal and element techniques and interface elements. *International Journal of Fracture,* 161**,** 97-119.

Dvorkin, E. N., Cuitiño, A. M. & Gioia, G. 1990. Finite elements with displacement interpolated embedded localization lines insensitive to mesh size and distortions. *International Journal for Numerical Methods in Engineering,* 30**,** 541-564.

Fib 2013. *Model Code for Concrete Structures 2010*, Wiley-VCH Verlag GmbH & Co. KGaA.

Graça-e-Costa, R., Alfaiate, J., Dias-da-Costa, D., Neto, P. & Sluys, L. J. 2013. Generalisation of non-iterative methods for the modelling of structures under non-proportional loading. *International Journal of Fracture,* 182**,** 21-38.

Graça-e-Costa, R., Alfaiate, J., Dias-da-Costa, D. & Sluys, L. J. 2012. A non-iterative approach for the modelling of quasi-brittle materials. *International Journal of Fracture,* 178**,** 281-298.

Gutiérrez, M. A. 2004. Energy release control for numerical simulations of failure in quasi-brittle solids. *Communications in Numerical Methods in Engineering,* 20**,** 19-29.

Jirásek, M. & Zimmermann, T. 2001. Embedded crack model: Part I. basic formulation. *International Journal for Numerical Methods in Engineering,* 50**,** 1269-1290.

Linder, C. & Armero, F. 2007. Finite elements with embedded strong discontinuities for the modeling of failure in solids. *International Journal for Numerical Methods in Engineering,* 72**,** 1391-1433.

Moës, N., Dolbow, J. & Belytschko, T. 1999. A finite element method for crack growth without remeshing. *International Journal for Numerical Methods in Engineering,* 46**,** 131-150.

Oliver, J. 1996. Modelling strong discontinuities in solid mechanics via strain softening constitutive equations. Part 2: Numerical simulation. *International Journal for Numerical Methods in Engineering,* 39**,** 3601-3623.

Simo, J. C. & Rifai, M. S. 1990. A class of mixed assumed strain methods and the method of incompatible modes. *International Journal for Numerical Methods in Engineering,* 29**,** 1595-1638.

Verhoosel, C. V., Remmers, J. J. C. & Gutiérrez, M. A. 2009. A dissipation-based arc-length method for robust simulation of brittle and ductile failure. *International Journal for Numerical Methods in Engineering,* 77**,** 1290-1321.

Wells, G. N. & Sluys, L. J. 2001a. A new method for modelling cohesive cracks using finite elements. *International Journal for Numerical Methods in Engineering,* 50**,** 2667-2682.

Wells, G. N. & Sluys, L. J. 2001b. Three-dimensional embedded discontinuity model for brittle fracture. *International Journal of Solids and Structures,* 38**,** 897-913.